

Mapping quantum chemical dynamics problems onto spin-lattice simulators

Debadrita Saha, Srinivasan S. Iyengar ^a

*Department of Chemistry and Department of Physics,
Indiana University, 800 E. Kirkwood Ave, Bloomington, IN-47405*

Philip Richerme^b

*Department of Physics, Indiana University,
800 E. Kirkwood Ave, Bloomington, IN-47405*

Jeremy M. Smith

*Department of Chemistry, Indiana University,
800 E. Kirkwood Ave, Bloomington, IN-47405*

Amr Sabry

*Department of Computer Science, School in Informatics,
Computing and Engineering, Indiana University,
800 E. Kirkwood Ave, Bloomington, IN-47405*

(Dated: February 20, 2022)

^a Email: iyengar@indiana.edu

^b Email: richerme@indiana.edu

The accurate computational determination of chemical, materials, biological, and atmospheric properties has critical impact on a wide range of health and environmental problems, but is deeply limited by the computational scaling of quantum-mechanical methods. The complexity of quantum-chemical studies arises from the steep algebraic scaling of electron correlation methods, and the exponential scaling in studying nuclear dynamics and molecular flexibility. Together these represent a grand challenge to modern computational chemistry. Here we provide an approximate algorithm that allows the quantum dynamical time-evolution of nuclei on a Born-Oppenheimer surface by mapping these to a spin-lattice quantum simulator. Using a pre-computed Hamiltonian that describes quantum nuclear dynamics, we directly determine the local fields and spin-spin couplings needed to control Ising-type spin-lattice dynamics which emulate the time evolution of the molecular system. The map is demonstrated for a short-strong hydrogen bonded system of significance in a range of chemical problems.

The quantum mechanical treatment of electrons and nuclei is critical for a wide range of problems that are of significance to biological, materials, and atmospheric studies. For example, hydrogen transfer processes are ubiquitous in reactions critical to human health, alternative energy sources, food security and environmental remediation¹. Yet, the detailed treatment of such problems is confounded by the presence of non-trivial quantum nuclear effects, such as hydrogen tunneling², coupled with electron correlation³. For the study of electron correlation in most molecular systems, classical approximations can provide significant speedups compared to exponentially-scaling full-configuration interaction calculations. Indeed, chemical accuracy may be obtained for many systems using the well-known CCSD(T) method⁴ that has an associated scaling cost of $\mathcal{O}(N^{6-7})$, where N represents the number of electrons. More recently, algorithms to solve electron correlation problems in small molecular systems have been implemented on quantum hardware devices using trapped atomic ions, photons, nuclear spins, quantum dots, Rydberg atoms, and superconducting circuits⁵⁻¹⁶.

The mapping of most electron correlation problems onto quantum hardware is enabled through Jordan-Wigner transformations^{17,18}, in which a product of Fermionic creation and annihilation operators can be transformed to a chain of Pauli spin operators. In contrast, the intrinsic spin statistics of quantum nuclear dynamics problems do not play a role under conditions prevalent in biological, materials, and atmospheric systems, such as hydrogen transfer reactions under ambient

conditions. As a result, most such quantum dynamics studies are currently constructed using basis sets and on grids. Furthermore, many of these problems are known to display anomalous nuclear quantum effects^{2,19,20} that are challenging to study due to the aforementioned exponential cost of quantum dynamics with increasing degrees of freedom. Unlike several recent attempts on the electron correlation problem^{5–16}, no efficient method of solving or approximating quantum nuclear dynamics problems on quantum computing hardware has been found to date.

The primary goal of this paper is to develop a set of mapping protocols to effect the study of quantum nuclear dynamics on quantum hardware. We provide and analyse an approximate algorithm to map exponentially-scaling quantum nuclear dynamics problems on a single Born–Oppenheimer surface onto a generalized Ising-model Hamiltonian. Since such problems do not need to be encoded using a set of Fermionic operators, we do not write the Ising model and molecular Hamiltonian in their respective second quantized forms. Instead, we first probe the structure of the Ising Hamiltonian matrix in its exponential scaling-space of spin basis vectors. This exponential space is admittedly intractable. Yet, our analysis of the Ising Hamiltonian matrix reveals an intrinsic structure where specific blocks appear within the Ising Hamiltonian matrix, and the corresponding matrix elements are only controlled by a subset of the externally controlled field parameters that dictate the dynamics of the model. To the best of our knowledge, such a structure has never been noted, or exploited, before in the literature. This structure allows us to characterise the general class of problems that may be “computable” using such hardware systems and in this paper we further inspect the extent to which quantum chemical dynamics studies may be conducted on such systems, when the statistics of particle permutation need not be included.

Such Ising-type Hamiltonians may be implemented on a range of quantum computing platforms, such as ion-traps^{21,22}, super-conducting coils²³, Bosonic processors with photons^{24–26}, solid state devices and quantum dots inside cavities^{27–30}, and Rydberg atoms^{31,32}. For specificity, we will illustrate our mapping protocols for ion-trap based quantum architectures, in which ions form defect-free arrangements and can support quantum coherence times longer than 10 minutes³³. Interactions between ions map to interactions between effective quantum spin states and quantum-harmonic-oscillator bath states – each of which can be precisely controlled and programmed using laser light³⁴. Site-resolved detection of each ion’s spin state can be achieved with near-unit fidelity³⁵. These features have made trapped ions the leading platform for establishing atomic frequency standards³⁶ and one of the leading candidates for performing quantum simulations and quantum computations

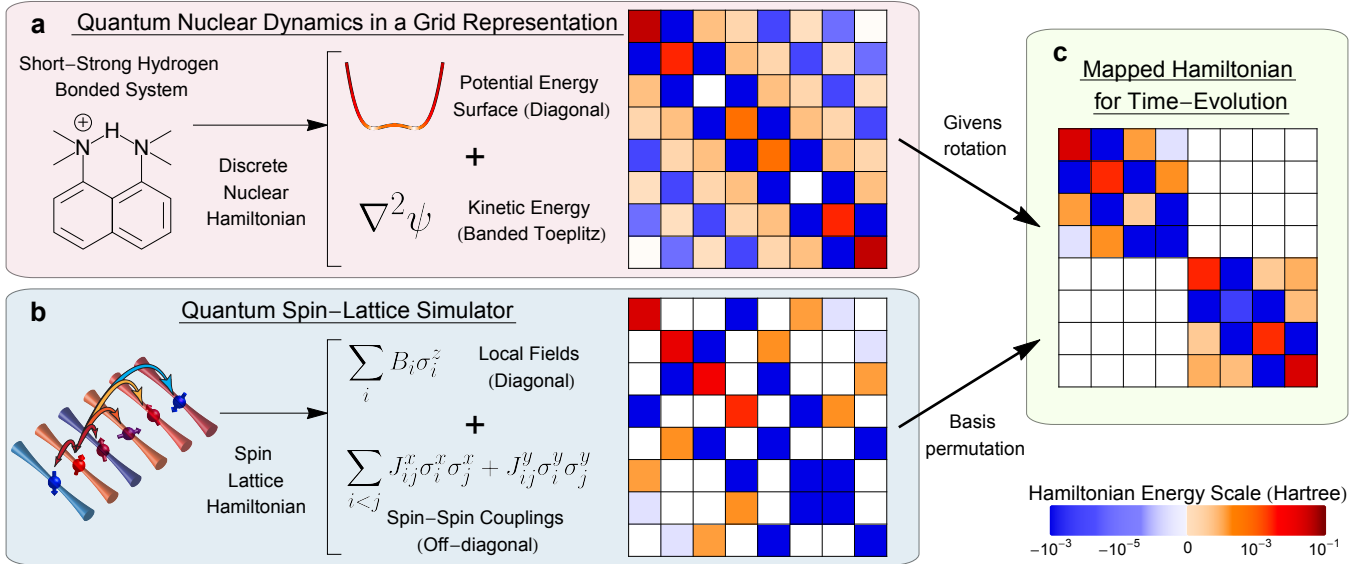


FIG. 1. An outline of the mapping algorithm. The algorithm converts the Born-Oppenheimer potential surface and kinetic energy terms in a quantum-nuclear problem to a set of controllable parameters and facilitates the dynamical evolution of quantum states in an ion-trap. Box (a) shows the Born-Oppenheimer potential and kinetic energies for a short-strong hydrogen bonded system. This system Hamiltonian is mapped onto an ion trap quantum simulator shown in box (b). Discrete representation of the nuclear Hamiltonian and appropriate rotations yield ion-trap parameters, $\{B_i^z\}; \{J_{ij}^x, J_{ij}^y\}$, to determine the Ising model used to control the dynamics of lattice spin-states.

on such interacting spin systems.^{22,37-42}

The mapping algorithm is illustrated in Figure 1. The specific family of targeted problems involves the description of nuclear dynamics on a single Born-Oppenheimer state. An example of such a problem is shown in Figure 1a, where we depict a system containing a short-strong hydrogen bond with anharmonic vibrational behavior along the donor-acceptor axis. This problem is prototypical and is representative of a broad range of systems that occur during hydrogen transfer reactions² and in hydrogen-bonded systems that are known to have significance in many critical processes¹. We pre-compute the Born-Oppenheimer potential using electronic structure calculations and obtain a discrete version of the quantum nuclear Hamiltonian. To map this Hamiltonian onto a spin-lattice model, the key insights in this paper are as follows: (i) A projected subspace of a specific unitary transformation of the diagonal elements of the quantum nuclear Hamiltonian (related to the Born-Oppenheimer potential) maps to and defines the local magnetic fields applied on each

lattice site of an Ising model Hamiltonian. (ii) A similarly projected subspace of a related unitary transformation of the off-diagonal elements of the quantum nuclear Hamiltonian (related to the nuclear kinetic energy operator) defines and is mapped onto the inter-site coupling terms in the Ising model. Thus, we take a critical step towards solving quantum nuclear dynamics problems, and more generally problems that may not obey Fermi statistics, by mapping them to Ising-type Hamiltonians realizable on ion-trap quantum hardware.

Block structure of Ising-type Hamiltonians: We first inspect the symmetry involved in such Hamiltonians to characterize the general class of mappable problems. We begin with a set of isolated qubits in alignment with the most commonly-used computing model today²². For ion-trap quantum hardware, the generalized Ising Hamiltonian is represented by a spin-lattice of qubits, where (a) the energy gap between the states at each qubit, i , are controlled by local effective magnetic fields, $\{B_i^x, B_i^y, B_i^z\}$, and (b) the spin-spin coupling between different lattice sites, i and j , is controlled using laser pulses, also spatially non-isotropic, and represented as $\{J_{ij}^x, J_{ij}^y, J_{ij}^z\}$. Thus, the most general Hamiltonian achievable within the ion trap quantum hardware at low temperatures is

$$\mathcal{H}_{IT} = \sum_{\gamma} \sum_{\substack{i=1 \\ j>i}}^{N-1} J_{ij}^{\gamma} \sigma_i^{\gamma} \sigma_j^{\gamma} + \sum_{\gamma} \sum_{i=1}^N B_i^{\gamma} \sigma_i^{\gamma} \quad (1)$$

where $\gamma \in (x, y, z)$, and N is the number of qubits (or ion-sites). The quantities $\{\sigma_i^{\gamma}\}$ are the Pauli spin operators acting on the i^{th} lattice site along the γ -direction of the Bloch sphere. Here, we map the Born-Oppenheimer nuclear Hamiltonian onto Eq. (1), thus allowing the two quantum systems to undergo analogous quantum dynamics. Towards this, the parameters $\{B_i^{\gamma}; J_{ij}^{\gamma}\}$ are “programmed” as per the elements of the classically determined Born-Oppenheimer nuclear Hamiltonian matrix.

To arrive at such a map, we first examine the intrinsic symmetries that are present within generalized Ising Hamiltonians. The ion-trap Hamiltonian, \mathcal{H}_{IT} , is naturally represented in a basis of 2^N spin states. To gauge the set of mappable problems, we introduce a general set of permutations on the spin basis vectors to reveal a novel block structure of the Ising Hamiltonian matrix. Specifically, the 2^N spin states are partitioned into two subsets created from the span of vectors arising from the action of even, $\{\mathbf{S}^{+2n}\}$, and odd, $\{\mathbf{S}^{+2n-1}\}$, total spin raising operators, on the total down-spin state, $|\downarrow\downarrow\downarrow\cdots\rangle$. The resultant block form of the Ising model Hamiltonian (Figure 1c) is a critical general result in this paper. Specifically, the matrix that determines the time-evolution of the hardware system separates into two blocks that can only be coupled by turning on $\{B_i^x; B_i^y\}$. Thus eliminating these fields would yield two separate blocks allowing the treatment of systems that may

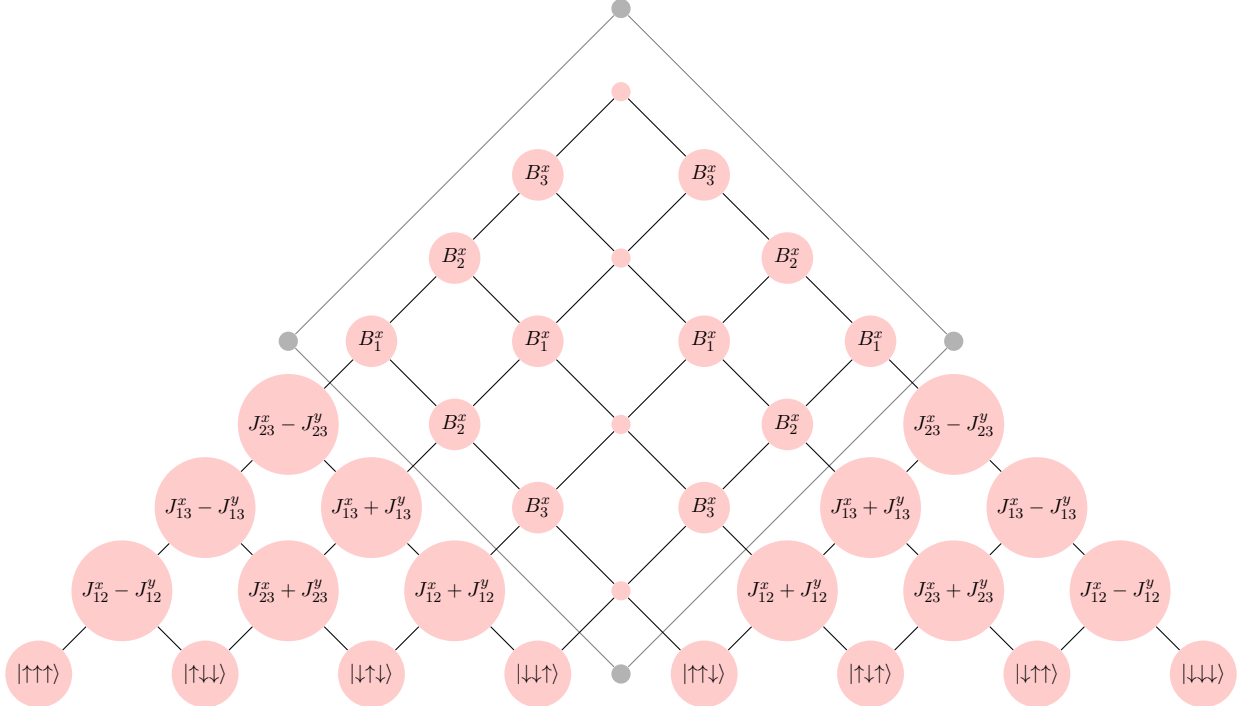


FIG. 2. **Block structure of the ion-trap Hamiltonian for a three qubit system.** Computational (spin) basis state kets are presented at the base of the figure. These states are partitioned into odd, $\{\mathbf{S}^{+2n-1}\}$, and even, $\{\mathbf{S}^{+2n}\}$, spans of the total spin raising operators. The interaction between any two states, $|i\rangle$ and $|j\rangle$ is the ij^{th} matrix element of the ion trap Hamiltonian. For example, $\langle \uparrow\downarrow\uparrow | \mathcal{H}_{IT} | \downarrow\downarrow\downarrow \rangle \equiv [J_{13}^x - J_{13}^y]$. The off-diagonal block is marked in gray.

have a similar block structure. Similarly, the off-diagonal matrix elements within each block are determined by the laser field parameters, $\{J_{ij}^x; J_{ij}^y\}$. (See Figure 2.)

Mapping protocols for quantum chemical dynamics: The structure of the ion-trap Hamiltonian constrains the class of mappable problems. These constraints dictate the accuracy to which quantum chemical dynamics simulations can be performed on an ion-trap system given by Eq. (1). Due to the structure discussed above, the diagonal elements of mappable Hamiltonians and off-diagonal parts of each individual block are Hadamard transformed to provide $\{B_i^z; J_{ij}^z\}$ and $\{J_{ij}^x; J_{ij}^y\}$, respectively. Similarly the coupling between blocks in the Ising Hamiltonian, are controlled through $\{B_i^x; B_i^y\}$ and provide handles for the appropriate blocks of mappable Hamiltonians. However, these maps are not exact for arbitrary Hamiltonians, beyond three-qubits, and in the Methods section we provide error-bounds to determine the extent to which the Ising Hamiltonians

deviate from the molecular Hamiltonian (or any other general matrix). Thus our quantum nuclear dynamics test case, that will be mapped to the aforementioned Ising Hamiltonian, exploits this block structure. We illustrate the map by studying a symmetric hydrogen bonded system displayed in Figure 1a, where a symmetric double-well potential is also shown. The kinetic energy operator is represented in a banded-Toeplitz form using Distributed Approximating Functionals (DAFs)⁴³; the potential is pre-computed classically using electronic structure calculations. The resultant molecular Hamiltonian is further unitary transformed with a product of Givens rotations, to yield a block diagonal form, which allows us to exclude $\{B_i^x; B_i^y\}$ in the current treatment. Thus, both Hamiltonians, by construction, take the form depicted in Figure 1c.

Performance of the mapping protocol: We examine the map by classically simulating the quantum chemical dynamics and ion-trap dynamics independently. In doing so we study the evolution of the states prepared in the appropriate representations as governed by the Ising and molecular Hamiltonians, respectively. As stated, the parameters in the Ising Hamiltonian are determined, and thus controlled, by the pre-computed matrix elements of the molecular system. The specific intramolecular proton transfer problem considered here is that in protonated 1,8-bis(dimethylamino) naphthalene (DMANH⁺). The DMANH⁺ system has been frequently studied as a model for short, low-barrier hydrogen bonds that have a role in certain enzyme-catalyzed reactions. In solution, proton motion in DMANH⁺ is described by a low-barrier double-well potential, with barrier height influenced by solvent and temperature.^{44,45} The transition state corresponding to this proton transfer reaction has the hydrogen symmetrically placed between the donor and acceptor nitrogen atoms (Figure 1a). We treat the shared proton stretch dimension within the Born-Oppenheimer limit. The nuclear Hamiltonian is determined by the ground electronic state potential energy surface.

Given the block structure of both Hamiltonians, the initial wavepacket for the ion-trap system is chosen as a coherent linear combination of the spin states: $\left\{ \frac{|\uparrow\uparrow\uparrow\rangle + |\downarrow\downarrow\downarrow\rangle}{\sqrt{2}} \right\}$. Given the block structure of the Ising Hamiltonian with $\{B_i^x, B_i^y\}$ turned off, the components of this initial state, $|\uparrow\uparrow\uparrow\rangle$ and $|\downarrow\downarrow\downarrow\rangle$, are not coupled. Additionally, these states will not couple such as might be the case in the presence of B_3^x : for example, pathways such as $|\downarrow\downarrow\downarrow\rangle \xrightarrow{B_3^x} |\uparrow\downarrow\downarrow\rangle \xrightarrow{J_{12}^x - J_{12}^y} |\uparrow\uparrow\uparrow\rangle$ will remain unpopulated. Hence, in essence, $|\uparrow\uparrow\uparrow\rangle$ gets propagated as per the unitary evolution corresponding to the top diagonal block of the Ising Hamiltonian and $|\downarrow\downarrow\downarrow\rangle$ as per the bottom-block. This critical feature allows us to treat the two separated blocks as arising from two different ion-traps with two different sets of $\{B_i^\gamma; J_{ij}^\gamma\}$ parameters. In an analogous fashion to the ion-trap, the initial

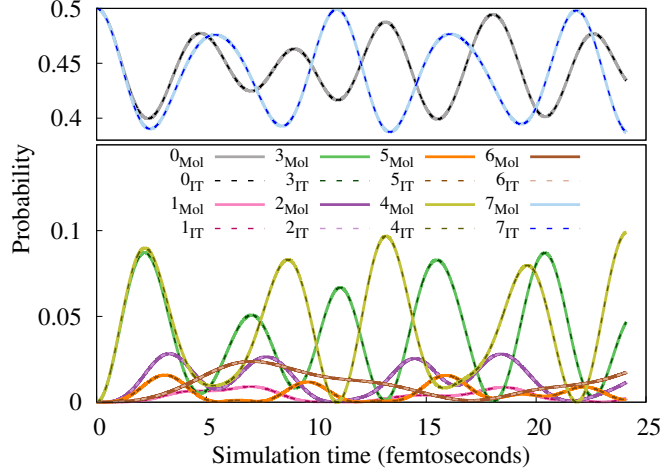


FIG. 3. Dynamics of the molecular and the ion trap systems. The integers depict the projections of a propagated state onto the i^{th} permuted spin basis states and the corresponding Givens transformed grid basis states for the ion-trap (dashed) and the molecular system (solid) respectively. Note that all propagations are conducted on classical platforms. The agreement of the quantum dynamics in both systems is exact to within numerical round-off (10^{-15}). The two rows in the figure legend represent the two sets spanned by odd and even spin raising operators, $\{\mathbf{S}^+\}$. An extended set of longer term dynamics results is provided in the Methods section.

wavepacket for the quantum nuclear dynamics problem is chosen as a Givens transform of a state localized closer to one of the nitrogen atoms in Figure 1a. Thus, through the map proposed above, we not only map the matrix elements, we also map the basis sets for the molecular system and the spin-lattice.

The spin-lattice and molecular wavepackets are then independently propagated and compared to gauge accuracy of the quantum simulation. The time-evolved wavepackets are projected onto the computational basis for the ion-trap and onto the grid representation for the quantum nuclear dynamics problem, and the resultant probability amplitudes are presented in Figures 3. The probabilities match exactly, apart from numerical round-off error (10^{-15}), for the quantum simulation of the dynamics of the two systems. Given the exact match between the spin-lattice dynamics and the quantum chemical dynamics, the features present in ion-trap dynamics must also exist in the chemical dynamics problem. Thus through the isomorphism constructed above, our algorithm allows the ability to probe any entanglement that may be present in chemical systems.

Outlook: The successful simulation of quantum nuclear dynamics on quantum hardware promises

a new paradigm for studying a broader class of coupled electron nuclear transfer problems. The next steps include inspection of nuclear wavepacket basis set dependence on the accuracy of the map. Using appropriate basis sets, it may be possible to reduce the number of independent descriptors within the molecular Hamiltonian, thus tailoring the accuracy of the map according to the constraints given in the Methods section. Furthermore, we will also consider qudit generalizations to Eq. (1) to allow an increase in the number of Ising-type control parameters. These studies can also be further extended to the study of condensed phase quantum dynamics where the interaction of the system with the environment variables is crucial for studying the dynamics of the coupled electron nuclear dynamics. These problems form a subset of dissipative quantum systems that can be approximately partitioned using spin-Boson Hamiltonians. In a complementary fashion, the full ion-trap Hamiltonian can also be partitioned into system-bath format with the addition of the phononic vibrational modes as the bath and the coupling between the qubits and these modes as system-bath interaction. This will provide us with more controllable parameters of the quantum hardware which could be exploited to map and study the dynamics of a larger class of chemical, bio-chemical and materials problems thus allowing the simulation of quantum nuclear dynamics on quantum hardware systems and novel quantum technologies.

Acknowledgment: This research was supported by the National Science Foundation grant OMA-1936353 to SSI, PR, JMS and AS. The authors are grateful to Dr. Miguel Angel Lopez Ruiz for valuable comments.

¹ Weinberg, D. R. *et al.* Proton-coupled electron transfer. *Chem. Rev.* **112**, 4016–4093 (2012).

² Nagel, Z. & Klinman, J. Tunneling and dynamics in enzymatic hydride transfer. *Chem. Rev.* **106**, 3095 (2006).

³ Hammes-Schiffer, S. Catalysts by design: The power of theory. *Acc. Chem. Res.* **50**, 561–566 (2017).

⁴ Raghavachari, K., Trucks, G. W., Pople, J. A. & Head-Gordon, M. A fifth-order perturbation comparison of electron correlation theories. *Chem. Phys. Lett.* **157**, 479–483 (1989).

⁵ O’Malley, P. J. J. *et al.* Scalable quantum simulation of molecular energies. *Phys. Rev. X* **6**, 031007 (2016).

⁶ Kandala, A. *et al.* Hardware-efficient variational quantum eigensolver for small molecules and quantum

magnets. *Nature* **549**, 242 (2017).

⁷ Xia, R. & Kais, S. Quantum machine learning for electronic structure calculations. *Nat. Commun.* **9**, 4195 (2018).

⁸ Gorman, D. J. *et al.* Engineering vibrationally assisted energy transfer in a trapped-ion quantum simulator. *Phys. Rev. X* **8**, 011038 (2018).

⁹ Nam, Y. *et al.* Ground-state energy estimation of the water molecule on a trapped ion quantum computer. *npj Quantum Inf.* **6**, 33 (2020).

¹⁰ Wang, B.-X. *et al.* Efficient quantum simulation of photosynthetic light harvesting. *npj Quantum Inf.* **4** (2018).

¹¹ Chin, A. W., Mangaud, E., Atabek, O. & Desouter-Lecomte, M. Coherent quantum dynamics launched by incoherent relaxation in a quantum circuit simulator of a light-harvesting complex. *Phys. Rev. A* **97** (2018).

¹² Potocnik, A. *et al.* Studying light-harvesting models with superconducting circuits. *Nat. Commun.* **9** (2018).

¹³ Peruzzo, A. *et al.* A variational eigenvalue solver on a photonic quantum processor. *Nat. Commun.* **5**, 4213 (2014).

¹⁴ Grimsley, H. R., Economou, S. E., Barnes, E. & Mayhall, N. J. An adaptive variational algorithm for exact molecular simulations on a quantum computer. *Nat. Commun.* **10**, 1–9 (2019).

¹⁵ Arute, F. *et al.* Hartree-fock on a superconducting qubit quantum computer. *Science* **369**, 1084–1089 (2020).

¹⁶ Parrish, R. M., Hohenstein, E. G., McMahon, P. L. & Martinez, T. J. Quantum Computation of Electronic Transitions Using a Variational Quantum Eigensolver. *Phys. Rev. Lett.* **122** (2019).

¹⁷ Jordan, P. & Wigner, E. Über das paulische Äquivalenzverbot. *Z. Phys.* **47**, 631–651 (1928).

¹⁸ Ortiz, G., Gubernatis, J. E., Knill, E. & Laflamme, R. Quantum algorithms for fermionic simulations. *Phys. Rev. A* **64**, 022319 (2001).

¹⁹ Iyengar, S. S., Sumner, I. & Jakowski, J. Hydrogen tunneling in an enzyme active site: A quantum wavepacket dynamical perspective. *J. Phys. Chem. B* **112**, 7601 (2008).

²⁰ Sumner, I. & Iyengar, S. S. Analysis of hydrogen tunneling in an enzyme active site using von neumann measurements. *J. Chem. Theory Comput.* **6**, 1698 (2010).

²¹ Porras, D. & Cirac, J. I. Effective quantum spin systems with trapped ions. *Phys. Rev. Lett.* **92**, 207901

(2004).

²² Richerme, P. *et al.* Non-local propagation of correlations in quantum systems with long-range interactions. *Nature* **511**, 198–201 (2014).

²³ Barends, R. *et al.* Superconducting quantum circuits at the surface code threshold for fault tolerance. *Nature* **508**, 500–503 (2014).

²⁴ Lanyon, B. P. *et al.* Towards quantum chemistry on a quantum computer. *Nat. Chem.* **2**, 106–111 (2010).

²⁵ Aspuru-Guzik, A. & Walther, P. Photonic quantum simulators. *Nat. Phys.* **8**, 285–291 (2012).

²⁶ Knill, E., Laflamme, R. & Milburn, G. J. A scheme for efficient quantum computation with linear optics. *Nature* **409**, 46–52 (2001).

²⁷ Pellizzari, T., Gardiner, S. A., Cirac, J. I. & Zoller, P. Decoherence, continuous observation, and quantum computing: A cavity qed model. *Phys. Rev. Lett.* **75**, 3788 (1995).

²⁸ Loss, D. & DiVincenzo, D. P. Quantum computation with quantum dots. *Phys. Rev. A* **57**, 120 (1998).

²⁹ Imamog, A. *et al.* Quantum information processing using quantum dot spins and cavity qed. *Phys. Rev. Lett.* **83**, 4204 (1999).

³⁰ Calarco, T., Datta, A., Fedichev, P., Pazy, E. & Zoller, P. Spin-based all-optical quantum computation with quantum dots: Understanding and suppressing decoherence. *Phys. Rev. A* **68**, 012310 (2003).

³¹ Saffman, M., Walker, T. G. & Mølmer, K. Quantum information with rydberg atoms. *Rev. Mod. Phys.* **82**, 2313 (2010).

³² Bernien, H. *et al.* Probing many-body dynamics on a 51-atom quantum simulator. *Nature* **551**, 579–584 (2017).

³³ Wang, Y. *et al.* Single-qubit quantum memory exceeding ten-minute coherence time. *Nat. Photonics* **11**, 646 (2017).

³⁴ Mølmer, K. & Sørensen, A. Multiparticle entanglement of hot trapped ions. *Phys. Rev. Lett.* **82**, 1835 (1999).

³⁵ Noek, R. *et al.* High speed, high fidelity detection of an atomic hyperfine qubit. *Opt. Lett.* **38**, 4735–4738 (2013).

³⁶ Ludlow, A. D., Boyd, M. M., Ye, J., Peik, E. & Schmidt, P. O. Optical atomic clocks. *Rev. Mod. Phys.* **87**, 637 (2015).

³⁷ Blatt, R. & Roos, C. F. Quantum simulations with trapped ions. *Nat. Phys.* **8**, 277 (2012).

³⁸ Islam *et al.*, R. Emergence and frustration of magnetism with variable-range interactions in a quantum simulator. *Science* **340**, 583–587 (2013).

³⁹ Richerme, P. *et al.* Experimental performance of a quantum simulator: Optimizing adiabatic evolution and identifying many-body ground states. *Phys. Rev. A* **88**, 012334 (2013).

⁴⁰ Senko, C. *et al.* Coherent imaging spectroscopy of a quantum many-body spin system. *Science* **345**, 430–433 (2014).

⁴¹ Smith, J. *et al.* Many-body localization in a quantum simulator with programmable random disorder. *Nat. Phys.* **12**, 907 (2016).

⁴² Zhang *et al.*, J. Observation of a discrete time crystal. *Nature* **543**, 217 (2017).

⁴³ Kouri, D. J., Huang, Y. & Hoffman, D. K. Iterated real-time path integral evaluation using a distributed approximating functional propagator and average-case complexity integration. *Phys. Rev. Lett.* **75**, 49–52 (1995).

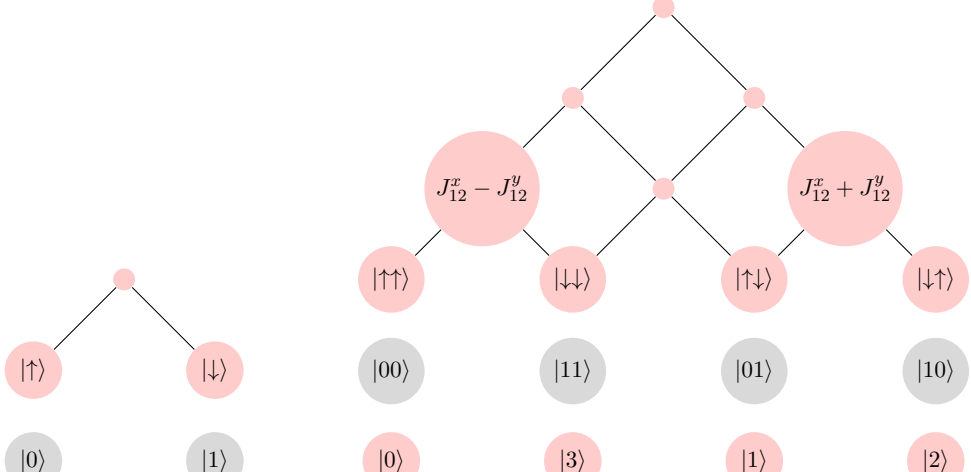
⁴⁴ Perrin, C. L. Are Short, Low-Barrier Hydrogen Bonds Unusually Strong? *Acc. Chem. Res.* **43**, 1550–1557 (2010).

⁴⁵ Pietrzak, M. *et al.* Symmetrization of Cationic Hydrogen Bridges of Protonated Sponges Induced by Solvent and Counteranion Interactions as Revealed by NMR Spectroscopy. *Chem. Eur. J.* **16**, 1679–1690 (2010).

METHODS

Block structure of Ising-type Hamiltonians obtained from computing the computational basis using spin operators: To arrive at a map between the molecular Hamiltonian for quantum nuclear dynamics and the Ising-type Hamiltonian in Eq. (1) we first examine the intrinsic symmetries that are present within generalized Ising Hamiltonians. This analysis also allows us to characterize the general class of mappable problems for these kinds of quantum hardware.

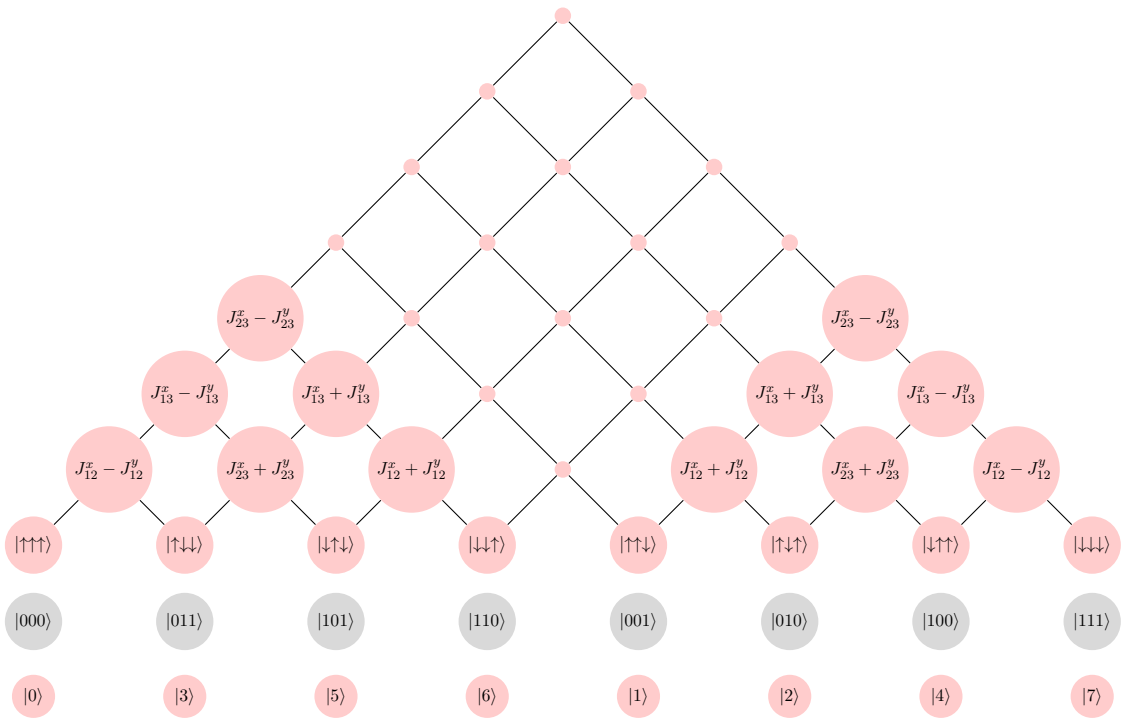
The ion-trap Hamiltonian, \mathcal{H}_{IT} , is naturally represented in a basis of 2^N spin states, where for example, $\{| \uparrow\uparrow \rangle, | \uparrow\downarrow \rangle, | \downarrow\uparrow \rangle, | \downarrow\downarrow \rangle\}$ form a basis for a 2-qubit system. These now provide us with a “computational basis” with programmable handles, $\{B_i^\gamma; J_{ij}^\gamma\}$. To gauge the set of mappable problems, we introduce a general set of permutations on the computational basis vectors to reveal a novel Block structure of the Ising Hamiltonian matrix. Specifically, the 2^N spin states are partitioned into two sets that are created by the span of even and odd total spin raising operators. When this is done the Ising model Hamiltonian acquires a block form. While the structure derived here is completely general, it is illustrated in Figure 2 for a 3-qubit system. Also see Figure 4 where the resultant block form is clarified. Towards this, the basis vectors created from using an even number of lattice-site spin raising operators, $\{S_i^+\}$ acting on the full downspin state, $|2^N - 1\rangle \equiv |11\cdots\rangle \equiv |\downarrow\downarrow\cdots\rangle$, yield the set, $\{|2^N - 1\rangle; S_i^+ S_j^+ |2^N - 1\rangle; S_i^+ S_j^+ S_k^+ S_l^+ |2^N - 1\rangle; \dots\}$, that are grouped as part of one block of the ion-trap Hamiltonian. Similarly, the states obtained using an odd number of raising operators: $\{S_i^+ |2^N - 1\rangle; S_i^+ S_j^+ S_k^+ |2^N - 1\rangle; \dots\}$ are grouped into a second block. Thus the two sets independently span $\{\mathbf{S}^{+2n} |11\cdots\rangle\}$ and $\{\mathbf{S}^{+2n-1} |11\cdots\rangle\}$, where \mathbf{S}^+ is the total spin raising operator. When the basis functions are sorted in this fashion, the Ising Hamiltonian in Eq. (1) in the main paper partitions into the block structure that is illustrated in Figure 2 for a 3-qubit system. This is further elaborated in Figure 4 where the bottom rows represent the sequence of the 2^N computational basis states grouped in the manner described above; the ket identities are defined using integer representations of the bit-sequences that represent the spin states. The nodes above the bottom rows represent the associated off-diagonal elements in the Ising-type Hamiltonian (Eq. (1)), that is the coupling between the computational basis states. As seen from Figure 2, the $\{J_{ij}^x; J_{ij}^y\}$ terms only couple the computational basis vectors inside the same block, that is basis vectors that span $\{|i\rangle \leftarrow \mathbf{S}^{+2n} |j\rangle\}$, whereas $\{B_i^x; B_i^y\}$ couple across the blocks that span $\{|i\rangle \leftarrow \mathbf{S}^{+2n-1} |j\rangle\}$. The diagonal elements of the matrix, not shown in the figure to maintain clarity, contain linear combinations of $\{B_i^z; J_{ij}^z\}$. This block-form of the Ising-type



(a) 1-qubit block

structure

(b) 2-qubit Block structure



(c) 3-qubit Block structure

FIG. 4. Complements Figure 2. At the base of each figure are the computational basis state kets. The interaction between any two states, $|i\rangle$ and $|j\rangle$ can be read off from the graph, by starting at the two states and following the lines to their intersection. The node at the intersection gives the interaction between the two. For example, $|2\rangle$ and $|7\rangle$ in Figure (c) have an off-diagonal matrix element of $[J_{13}^x - J_{13}^y]$. The blank nodes are zero, and show the block diagonal form of the Ising Hamiltonian when $\{B_i^x, B_i^y\}$ are set to zero.

Hamiltonian is a significant general result in this paper. To the best of our knowledge such a structure of the general Ising model has never been discussed in the literature, and as we find below, this analysis is critical towards mapping arbitrary problems.

Recursive, block structure of the Ising Hamiltonian matrix: The Ising Hamiltonian matrix, \mathbf{H}_N , for a spin-lattice containing N spin sites (Eq. (1)) when represented in the above classified computational basis: $\left\{ \left\{ \mathbf{S}^{+2n} |2^N - 1\rangle \right\}; \left\{ \mathbf{S}^{+2n-1} |2^N - 1\rangle \right\} \right\}$, may be recursively written in a blocked form as,

$$\mathbf{H}_N = \begin{bmatrix} \mathbf{H}_N^{\mathbf{D}1} & \mathbf{B}_N \\ \mathbf{B}_N^\dagger & \mathbf{H}_N^{\mathbf{D}2} \end{bmatrix} = \begin{bmatrix} \mathbf{H}_{N-1}^{\mathbf{D}1} + B_N^z \mathbf{I}_{2^{N-2}} + \mathbf{J}_{z,N}^1 & \mathbf{J}_{xy,N}^1 \\ \mathbf{J}_{xy,N}^1^\top & \mathbf{H}_{N-1}^{\mathbf{D}2} - B_N^z \mathbf{I}_{2^{N-2}} + \mathbf{J}_{z,N}^1 \\ \hline \mathbf{B}_{N-1}^\dagger & (B_N^x - iB_N^y) \mathbf{I}_{2^{N-2}} \\ (B_N^x + iB_N^y) \mathbf{I}_{2^{N-2}} & \mathbf{B}_{N-1} \end{bmatrix} \begin{bmatrix} \mathbf{B}_{N-1} & (B_N^x - iB_N^y) \mathbf{I}_{2^{N-2}} \\ (B_N^x + iB_N^y) \mathbf{I}_{2^{N-2}} & \mathbf{B}_{N-1} \end{bmatrix} \begin{bmatrix} \mathbf{H}_{N-1}^{\mathbf{D}2} + B_N^z \mathbf{I}_{2^{N-2}} + \mathbf{J}_{z,N}^2 & \mathbf{J}_N^2 \\ \mathbf{J}_{xy,N}^2^\top & \mathbf{H}_{N-1}^{\mathbf{D}1} + B_N^z \mathbf{I}_{2^{N-2}} + \mathbf{J}_{z,N}^2 \end{bmatrix} \quad (2)$$

where both the diagonal blocks $\mathbf{H}_N^{\mathbf{D}1}$ and $\mathbf{H}_N^{\mathbf{D}2}$, and the off-diagonal block \mathbf{B}_N are recursively defined above, and \mathbf{I}_{2^N} denotes an identity matrix of size 2^N . The $\mathbf{J}_{xy,N}^1$ and $\mathbf{J}_{xy,N}^2$ matrices that appear in the recursive definition of the diagonal blocks, labeled \mathbf{D}_1 and \mathbf{D}_2 respectively, contain intersite coupling of the N^{th} spin site with the remaining $N - 1$ sites. To arrive at the matrix elements belonging to $\mathbf{J}_{xy,N}^1$ and $\mathbf{J}_{xy,N}^2$ above, a bitwise XOR operation is constructed between the corresponding computational bases, $|\lambda\rangle$ and $|\lambda'\rangle$ coupled by the them. The XOR operation provides the identity of the spin sites where these computational basis vectors differ, that is when the spin states are flipped across $|\lambda\rangle$ and $|\lambda'\rangle$. When the bases differ at two spin lattice site locations, i and j , the corresponding matrix element of $\mathbf{J}_{xy,N}^1$ or $\mathbf{J}_{xy,N}^2$ is given by $J_{ij}^x \pm J_{ij}^y$. The phase preceding the corresponding J_{ij}^y values results from an XNOR operation on the i, j lattice sites discovered through the XOR operation above.

The terms, $\mathbf{J}_{z,N}^1$ and $\mathbf{J}_{z,N}^2$, in Eq. (2) are also defined in a similar fashion. Both $\mathbf{J}_{z,N}^1$ and $\mathbf{J}_{z,N}^2$ matrices are diagonal in form. Thus, the diagonal elements of $\mathbf{H}_N^{\mathbf{D}1}$ and $\mathbf{H}_N^{\mathbf{D}2}$ are incremented by a linear combination of all possible intersite couplings of the N^{th} spin site with the remaining $N - 1$ sites given by, $\sum_{i=1}^{N-1} (-1)^{\lambda_i \oplus \lambda_N} J_{iN}^z$.

As noted in the main paper, setting all the transverse local qubit magnetic fields, B_i^x and B_i^y to

zero in Eq. (1), yields a block-diagonal form which may be recursively written as,

$$\mathbf{H}_N = \begin{bmatrix} \mathbf{H}_{N-1}^{D1} + B_N^z \mathbf{I}_{2^{N-2}} & \mathbf{J}_{xy,N}^1 & \mathbf{0} & \mathbf{0} \\ \mathbf{J}_{xy,N}^1 \top & \mathbf{H}_{N-1}^{D2} - B_N^z \mathbf{I}_{2^{N-2}} & \mathbf{0} & \mathbf{0} \\ \mathbf{0} & \mathbf{0} & \mathbf{H}_{N-1}^{D2} + B_N^z \mathbf{I}_{2^{N-2}} & \mathbf{J}_{xy,N}^2 \\ \mathbf{0} & \mathbf{0} & \mathbf{J}_{xy,N}^2 \top & \mathbf{H}_{N-1}^{D1} - B_N^z \mathbf{I}_{2^{N-2}} + \mathbf{J}_{z,N}^2 \end{bmatrix} \quad (3)$$

At this stage it is critical to realize that the two blocks in the equation above are completely decoupled and basis vector components that undergo unitary evolution due to the top block are never influenced by elements from the bottom block and vice versa. This presents us with an additional degree of flexibility for our quantum simulation. We exercise this flexibility here and map separately the top and bottom blocks of the equation above, to two different N -qubit ion trap systems controlled by parameters $\{B_i^z; J_{ij}^\gamma\}$ and $\{\tilde{B}_i^z; \tilde{J}_{ij}^\gamma\}$ respectively. It is important to note here, that while the underlying structure of each block in the Ising Hamiltonian matrix remains the same, two different sets of ion-trap control parameters are used to simulate the top and bottom blocks respectively, thus providing greater flexibility in simulating real systems. We, therefore, introduce a subtle change in denoting the corresponding Ising model Hamiltonian as \mathcal{H}_N , and allow the diagonal blocks to be independently determined in the following manner:

$$\begin{aligned} \mathcal{H}_N &= \begin{bmatrix} \mathbf{H}_N^{D1} & \mathbf{0} \\ \mathbf{0} & \tilde{\mathbf{H}}_N^{D2} \end{bmatrix} \\ &= \begin{bmatrix} \mathbf{H}_{N-1}^{D1} + B_N^z \mathbf{I}_{2^{N-2}} & \mathbf{J}_{xy,N}^1 & \mathbf{0} & \mathbf{0} \\ (\mathbf{J}_{xy,N}^1) \top & \mathbf{H}_{N-1}^{D2} - B_N^z \mathbf{I}_{2^{N-2}} & \mathbf{0} & \mathbf{0} \\ \mathbf{0} & \mathbf{0} & \tilde{\mathbf{H}}_{N-1}^{D2} + \tilde{B}_N^z \mathbf{I}_{2^{N-2}} & \tilde{\mathbf{J}}_{xy,N}^2 \\ \mathbf{0} & \mathbf{0} & (\tilde{\mathbf{J}}_{xy,N}^2) \top & \tilde{\mathbf{H}}_{N-1}^{D1} - \tilde{B}_N^z \mathbf{I}_{2^{N-2}} + \tilde{\mathbf{J}}_{z,N}^2 \end{bmatrix} \end{aligned} \quad (4)$$

where the top-block is controlled by parameters, $\{B_i^z; J_{ij}^\gamma\}$, whereas the bottom block is controlled by a different set of ion-trap parameters, $\{\tilde{B}_i^z; \tilde{J}_{ij}^\gamma\}$. The molecular Hamiltonian is mapped to the above form of the Ising model Hamiltonian matrix.

We now illustrate the above form of Ising Hamiltonian for the 2- and 3-qubit systems. But, we note that the aforementioned basis set partitioning and Hamiltonian structure is completely general

and applies to all cases. Explicitly written, for the case of two-qubits, Eq. (4) takes the form

$$\mathcal{H}_2 = \begin{bmatrix} B_1^z + B_2^z + J_{12}^z & J_{12}^x - J_{12}^y & 0 & 0 \\ J_{12}^x - J_{12}^y & -B_1^z - B_2^z + J_{12}^z & 0 & 0 \\ 0 & 0 & \tilde{B}_2^z - \tilde{B}_1^z - \tilde{J}_{12}^z & \tilde{J}_{12}^x + \tilde{J}_{12}^y \\ 0 & 0 & \tilde{J}_{12}^x + \tilde{J}_{12}^y & \tilde{B}_1^z - \tilde{B}_2^z - \tilde{J}_{12}^z \end{bmatrix} \quad (5)$$

where again we have highlighted the distinction between ion-trap simulators that represent the top block, $\{B_i^z; J_{ij}^\gamma\}$, and those that control the bottom block, $\{\tilde{B}_i^z; \tilde{J}_{ij}^\gamma\}$. The three-qubit Hamiltonian is then recursively obtained from the two-qubit Hamiltonian as prescribed by Eq. (4) and may be written in compact form as follows:

$$\mathcal{H}_3 = \begin{bmatrix} \mathbf{H}_2^{\mathbf{D}1} + B_3^z \mathbf{I}_2 & \mathbf{J}_{\mathbf{xy},3}^1 & 0 & 0 \\ \mathbf{J}_{\mathbf{xy},3}^1 & \mathbf{H}_2^{\mathbf{D}2} - B_3^z \mathbf{I}_2 & 0 & 0 \\ 0 & 0 & \tilde{\mathbf{H}}_2^{\mathbf{D}2} + \tilde{B}_3^z \mathbf{I}_2 & \tilde{\mathbf{J}}_{\mathbf{xy},3}^2 \\ 0 & 0 & (\tilde{\mathbf{J}}_{\mathbf{xy},3}^2)^\top & \tilde{\mathbf{H}}_2^{\mathbf{D}1} - \tilde{B}_3^z \mathbf{I}_2 \end{bmatrix} \quad (6)$$

Here, $\mathbf{H}_2^{\mathbf{D}1}$ and $\mathbf{H}_2^{\mathbf{D}2}$ refer to the top and bottom diagonal blocks of the two-qubit Ising Hamiltonian (Eq. (3)) simulated using the ion-trap parameters $\{B_i^z; J_{ij}^\gamma\}$ while $\tilde{\mathbf{H}}_2^{\mathbf{D}1}$ and $\tilde{\mathbf{H}}_2^{\mathbf{D}2}$ refer to the top and bottom blocks of a the two-qubit Ising Hamiltonian (Eq.3) controlled by $\{\tilde{B}_i^z; \tilde{J}_{ij}^\gamma\}$. While most of $\mathbf{H}_2^{\mathbf{D}1}$ and $\mathbf{H}_2^{\mathbf{D}2}$ is preserved and appear as diagonal blocks of the 2 qubit Hamiltonian, the N^{th} qubit on-site term B_3^z , and intersite coupling terms with all $N - 1$ qubits J_{13}^z, J_{23}^z with appropriate phases are added to each diagonal element. The quantities, $\mathbf{J}_3^1, \mathbf{J}_3^2$ in the top block and $\tilde{\mathbf{J}}_3^1, \tilde{\mathbf{J}}_3^2$ in the bottom block capture the interaction of qubits 1 and 2 with qubit 3 in the form of the inter-site coupling terms for the two ion-traps respectively. Explicitly, the 3 qubit system Hamiltonian becomes:

$$\mathcal{H}_3 = \mathbf{H}_3^{\mathbf{D}1} \oplus \tilde{\mathbf{H}}_3^{\mathbf{D}2} \quad (7a)$$

where, for compactness we have written the ion-trap Hamiltonian as a direct sum of

$$\mathbf{H}_3^{\mathbf{D}1} = \begin{bmatrix} B_1^z + B_2^z + B_3^z & J_{12}^x - J_{12}^y & J_{13}^x - J_{13}^y & J_{23}^x - J_{23}^y \\ +J_{12}^z + J_{13}^z + J_{23}^z & +J_{12}^z - J_{13}^z - J_{23}^z & J_{23}^x + J_{23}^y & J_{13}^x + J_{13}^y \\ J_{12}^x - J_{12}^y & +J_{12}^z - J_{13}^z - J_{23}^z & J_{23}^x + J_{23}^y & J_{13}^x + J_{13}^y \\ J_{13}^x - J_{13}^y & J_{23}^x + J_{23}^y & -J_{12}^z + J_{13}^z - J_{23}^z & J_{12}^x + J_{12}^y \\ J_{23}^x - J_{23}^y & J_{13}^x + J_{13}^y & J_{12}^x + J_{12}^y & -J_{12}^z - J_{13}^z + J_{23}^z \end{bmatrix} \quad (7b)$$

$$\tilde{\mathbf{H}}_3^{\mathbf{D2}} = \begin{bmatrix} \tilde{B}_2^z - \tilde{B}_1^z + \tilde{B}_3^z & \tilde{J}_{12}^x + \tilde{J}_{12}^y & \tilde{J}_{13}^x + \tilde{J}_{13}^y & \tilde{J}_{23}^x - \tilde{J}_{23}^y \\ -\tilde{J}_{12}^z - \tilde{J}_{13}^z + \tilde{J}_{23}^z & \tilde{B}_1^z - \tilde{B}_2^z + \tilde{B}_3^z & \tilde{J}_{23}^x + \tilde{J}_{23}^y & \tilde{J}_{13}^x - \tilde{J}_{13}^y \\ \tilde{J}_{12}^x + \tilde{J}_{12}^y & -\tilde{J}_{12}^z + \tilde{J}_{13}^z - \tilde{J}_{23}^z & \tilde{J}_{23}^x + \tilde{J}_{23}^y & \tilde{J}_{13}^x - \tilde{J}_{13}^y \\ \tilde{J}_{13}^x + \tilde{J}_{13}^y & \tilde{J}_{23}^x + \tilde{J}_{23}^y & \tilde{B}_1^z + \tilde{B}_2^z - \tilde{B}_3^z + \tilde{J}_{12}^z - \tilde{J}_{13}^z - \tilde{J}_{23}^z & \tilde{J}_{12}^x - \tilde{J}_{12}^y \\ \tilde{J}_{23}^x - \tilde{J}_{23}^y & \tilde{J}_{13}^x - \tilde{J}_{13}^y & \tilde{J}_{12}^x - \tilde{J}_{12}^y & -\tilde{B}_1^z - \tilde{B}_2^z - \tilde{B}_3^z + \tilde{J}_{12}^z + \tilde{J}_{13}^z + \tilde{J}_{23}^z \end{bmatrix} \quad (7c)$$

We further clarify that the top-block, $\mathbf{H}_3^{\mathbf{D1}}$, is controlled by parameters $\{B_i^z; J_{ij}^y\}$ whereas the bottom block, $\tilde{\mathbf{H}}_3^{\mathbf{D1}}$, is controlled by $\{\tilde{B}_i^z; \tilde{J}_{ij}^y\}$.

Degrees of freedom in the Ising Hamiltonian: For a given number of qubits, N , the number of ion-trap handles in Eq. (1) that control various sectors of the Hamiltonian matrix scale as

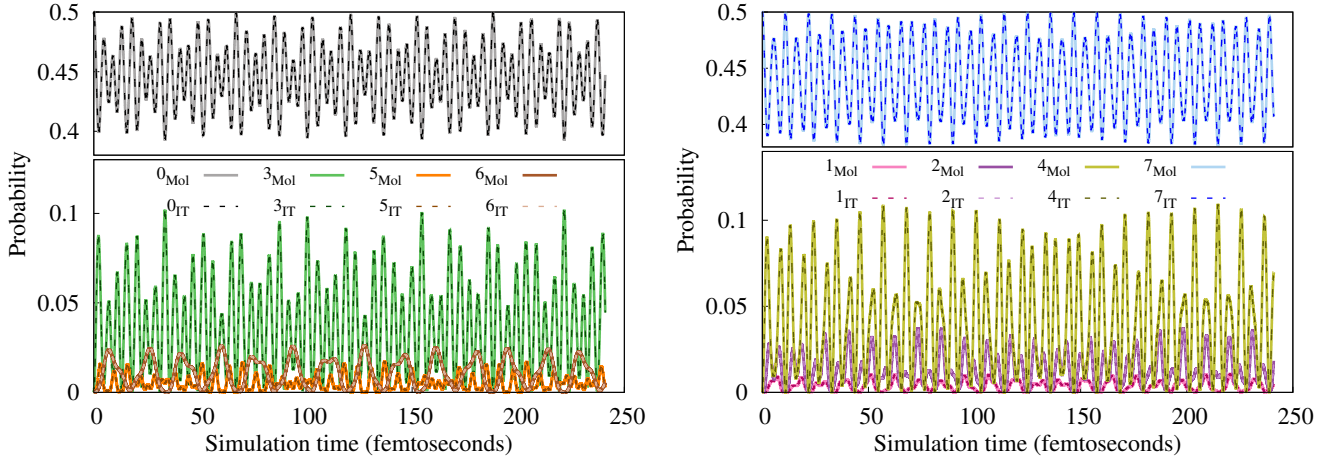
$$\{N + N(N - 1)/2\} + \{N(N - 1)\} + \{2N\} \rightarrow \mathcal{O}(N^2), \quad (8)$$

Here (a) the first quantity, $\{N + N(N - 1)/2\}$, refers to the parameters, $\{B_i^z; J_{ij}^z\}$, that control the diagonal elements of the matrix, (b) the second quantity on the left, $\{N(N - 1)\}$, refers to the parameters, $\{J_{ij}^x \pm J_{ij}^y\}$, that control the coupling between the basis vectors inside each block, and (c) finally $\{2N\}$ refers to the parameters, $\{B_i^x \pm iB_i^y\}$, that control the coupling across the sets of basis vectors created by using the odd and even raising operators described above. This characterization not only elucidates the degrees of freedom of the Ising model Hamiltonian in Eq. (1), but also provides the sectored availability of these control parameters.

At this stage there are two cases that become interesting insofar as mapping to realistic systems is concerned. In the first case, the structure of the Ising Hamiltonian is used as is, including the $\{B_i^x \pm iB_i^y\}$ terms, and the number of degrees of freedom is as given above and must match the same for the problem at hand to produce an accurate map. For the second case, if the $\{B_i^x \pm iB_i^y\}$ handles are eliminated, the system reduces to two separate blocks, that may be propagated independently, perhaps even on two different sets of ion-trap architectures arranged in parallel, or Trotterized on one single ion-trap architecture. It is this second case that we consider in this paper as it allows the ability to have different Ising model parameters for the two diagonal blocks, and in this case the number of ion-trap handles become:

$$2 \{N + N(N - 1)/2 + N(N - 1)\}. \quad (9)$$

which is, in fact, greater than the number of Ising model handles available in an $(N - 1)$ -qubit system when $N < 17$. The above discussion also implies that for Hamiltonians containing 2^N independent



(a)Projections of the time-dependent wavepackets onto Block I vectors (b)Projections of the time-dependent wavepackets onto Block II vectors

FIG. 5. The dynamics of the molecular system (solid) and the ion-trap system (dashed) that show their exact match to within numerical round-off (10^{-15}) over long simulation times sufficient to capture the molecular vibrational properties. Complements Figure 3 in the paper. The projection of the respective time-dependent wavepacket onto basis vectors within each of the two decoupled blocks are shown separately for clarity.

terms, only approximate computation is possible. In this sense, the current paper takes a first step towards providing the necessary accuracy bounds. (Precise error bounds are provided below.)

Propagation of the ion-trap lattice: Given the Hamiltonian in Eq. (4), the ion-trap hardware initial wavepacket state is directly propagated by the choice of $\{B_i^\gamma; J_{ij}^\gamma\}$ for arbitrary time-segments. In this publication we do not use a real ion-trap simulator, and hence we emulate the time-evolution by using the eigenstates of Eq. (4) in the corresponding time-evolution operator. The projection of the time-dependent wavepacket on the computational basis is shown using dashed lines in Figure 3 in the main paper and Figure 5 in this Methods section.

The grid based quantum nuclear Hamiltonian computed on classical hardware: The quantum nuclear Hamiltonian is constructed on classical hardware. For local potentials, the potential energy operator is diagonal in the coordinate representation. The kinetic energy may be approximated in a number of ways. One approach is to recognise that this operator is diagonal in the momentum representation and hence fast Fourier transforms are commonly employed⁷. In this

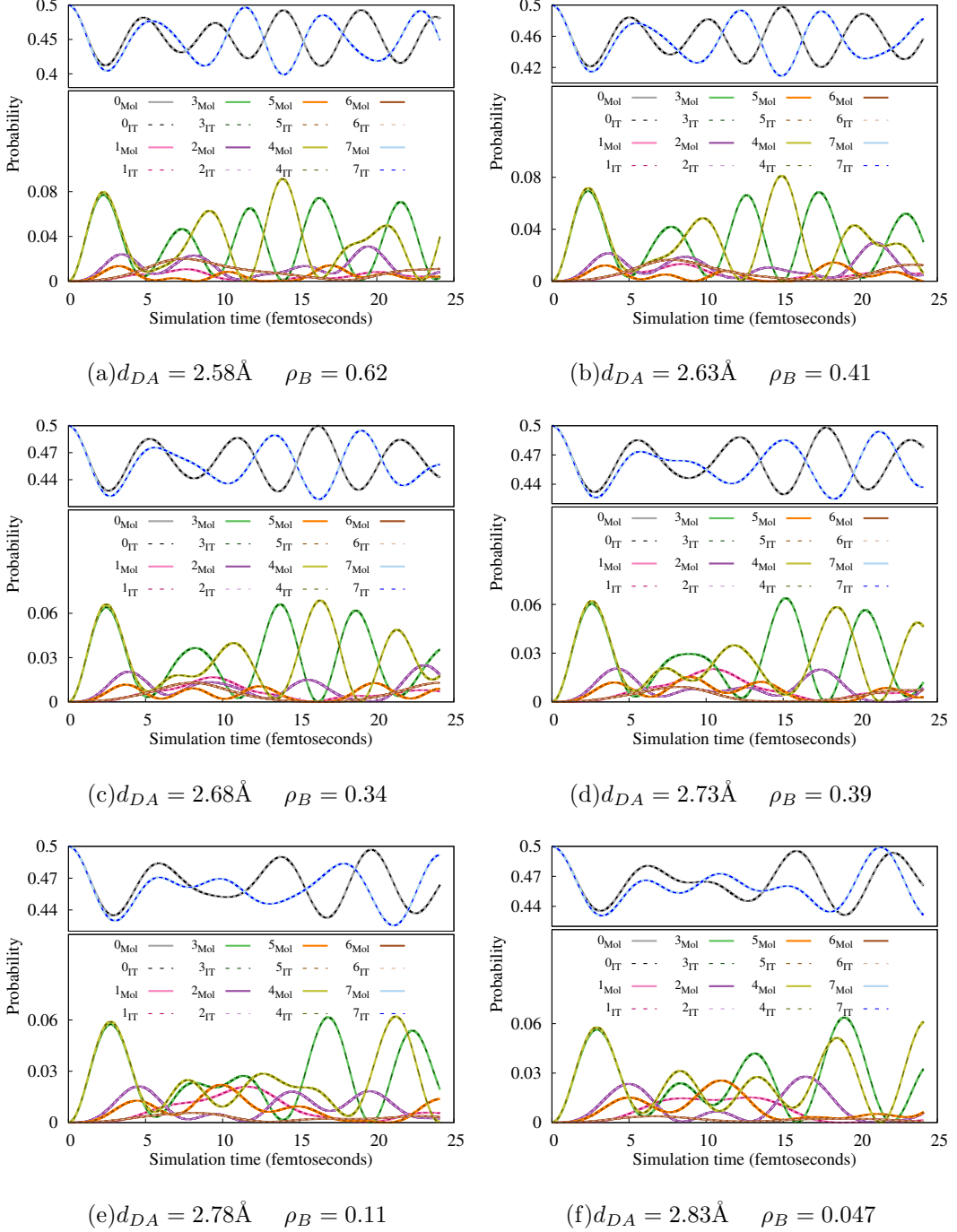


FIG. 6. Similar to Figure 3 but for multiple donor-acceptor distances (d_{DA}) between the nitrogen atoms for the molecule in Figure 1a. Boltzmann populations (ρ_B) are computed at 300K relative to the population of the configuration used in Figure 3, that has a d_{DA} value of 2.53 Å. The correlated changes in the $|0\rangle$ and $|7\rangle$ projections, are clearly facilitated by components along other basis vectors, and these may have a critical role on the reactive process as a function of temperature. The fact that the ion-lattice dynamics displays the same dynamical trends provides an additional probe to complex chemical systems.

paper, we employ an analytic banded, Toeplitz, distributed approximating functional (DAF)^{43?} representation for the coordinate space version the kinetic energy operator:

$$\tilde{K}(x, x') = \frac{-\hbar^2}{4m\sigma^3\sqrt{2\pi}} \exp\left\{-\frac{(x - x')^2}{2\sigma^2}\right\} \sum_{n=0}^{M_{DAF}/2} \left(\frac{-1}{4}\right)^n \frac{1}{n!} H_{2n+2}\left(\frac{x - x'}{\sqrt{2\sigma}}\right), \quad (10)$$

where $H_i(x)$ are the Hermite polynomials, x and x' are grid coordinates, and M_{DAF} and σ are parameters that together determine the accuracy and efficiency of the resultant approximate kinetic energy operator. Equation (10) uses the well-known analytical expression for free evolution of a Gaussian function⁷ along with the fact that the Hermite functions are generated from derivatives of Gaussian functions⁷. This yields an efficient propagation scheme to perform quantum dynamics and Feynman path integration⁷ through the action of a banded, sparse, Toeplitz matrix on a vector⁷.

In order to construct the potential surface for the intra-molecular hydrogen transfer in DMANH⁺ we locate the transition state with an imaginary frequency of the electronic structure Hessian matrix, with vibrational mode corresponding to the intra-molecular transfer direction corresponding to the shared hydrogen nuclear degrees of freedom. At this geometry, the shared proton is symmetrically located between the donor and acceptor nitrogen atoms. An intrinsic reaction coordinate calculation is used to verify that the transition state corresponded to the hydrogen transfer between the isoenergetic donor (reactant) and acceptor (product) states. These calculations are performed using standard electronic structure methods. The level of theory used is density functional theory for electrons with hybrid functional B3LYP and an atom-centered Gaussian basis set containing polarization and diffuse functions on all atoms, that is, 6-311++G(d,p). Future work will also including mapping of this Hamiltonian pre-computation step onto quantum hardware. A reduced dimensional potential energy surface calculation for one-dimensional proton motion along the donor-acceptor axis was performed at the transition state geometry. The surface is obtained on grid points symmetrically located along the donor-acceptor axis. We choose 2^N number of equally spaced grid points along this chosen dimension and perform electronic structure calculations at these points, on a classical computing platform, at the level of theory mentioned above, to obtain the one-dimensional potential energy surface for our system. The Hamiltonian for the molecular system in the grid basis is given by,

$$\langle x | \mathcal{H}^{Mol} | x' \rangle = \tilde{K}(x, x') + V(x) \quad (11)$$

where the potential energy is diagonal in the grid basis and the kinetic energy is expressed in terms of distributed approximating functionals, as per Eq. (10).

Unitary transformations that yield the Block structure of the nuclear Hamiltonian to make these commensurate with and mappable to the spin-lattice Hamiltonian: The nuclear Hamiltonian, $\mathcal{H}_{\text{Molecule}}$ from Eq. (11), has a banded Toeplitz structure due to the kinetic energy being expressed in terms of DAFs. The one-dimensional potential energy surface along the hydrogen transfer axis, $V(x)$ in Eq. (11), is a symmetric double well owing to the isoenergetic donor and acceptor sites arising from the symmetry of the system as may be clear from Figures 1a in the paper. We exploit the symmetric structure of the potential and the Toeplitz structure of the kinetic energy operator to construct a unitary transformation that block diagonalizes the nuclear Hamiltonian.

The unitary transform that leads to the block diagonalization of the nuclear Hamiltonian, to have a similar structure as the Ising Hamiltonian, can be expressed as a product of Givens rotations of the grid basis states. The effect of the Givens rotation on the grid basis states would be to create superposition states of symmetric grid basis states. The action of the product of Givens rotations is therefore, to yield a rotation in the 2^N dimensional basis state space, by a sequence of 2×2 (or one-qubit) rotations. This now divides the basis state space, in which the Hamiltonian is represented, into two sets of rotated states, created by the symmetric and anti-symmetric combinations, $\left\{ |\tilde{x}_i\rangle \equiv \frac{1}{\sqrt{2}} [|x_i\rangle \pm |x_{2^N+1-i}\rangle] \right\}$. These now form two mutually orthogonal subspaces to block diagonalize the nuclear Hamiltonian. This process is illustrated for a three-qubit system (2^3 -grid points) in Figure 7. The il^{th} matrix element of the resultant molecular Hamiltonian is thus explicitly written as

$$\tilde{\mathcal{H}}_{il}^{\text{Mol}} = \frac{1}{2} (\mathcal{H}_{i,l}^{\text{Mol}} + \alpha_l \mathcal{H}_{i,n+1-l}^{\text{Mol}} + \alpha_i \mathcal{H}_{n+1-i,l}^{\text{Mol}} + \alpha_i \alpha_l \mathcal{H}_{n+1-i,n+1-l}^{\text{Mol}}), \quad (12)$$

where $n = 2^N$ and $\alpha_i = \text{sgn}[i - (n+1)/2]$.

Quantum molecular dynamics propagation: Given the Givens transformed molecular Hamiltonian in Eq. (12), we determine the time-evolution by using the eigenstates of the transformed Hamiltonian in Eq. (4). The projection of the time-dependent wavepacket on the transformed grid basis, $\{|\tilde{x}\rangle\}$ is shown using solid lines in Figure 3 in the main paper and Figure 5 in this Methods section.

Obtaining the ion-trap parameters from the blocked nuclear Hamiltonian matrix ele-

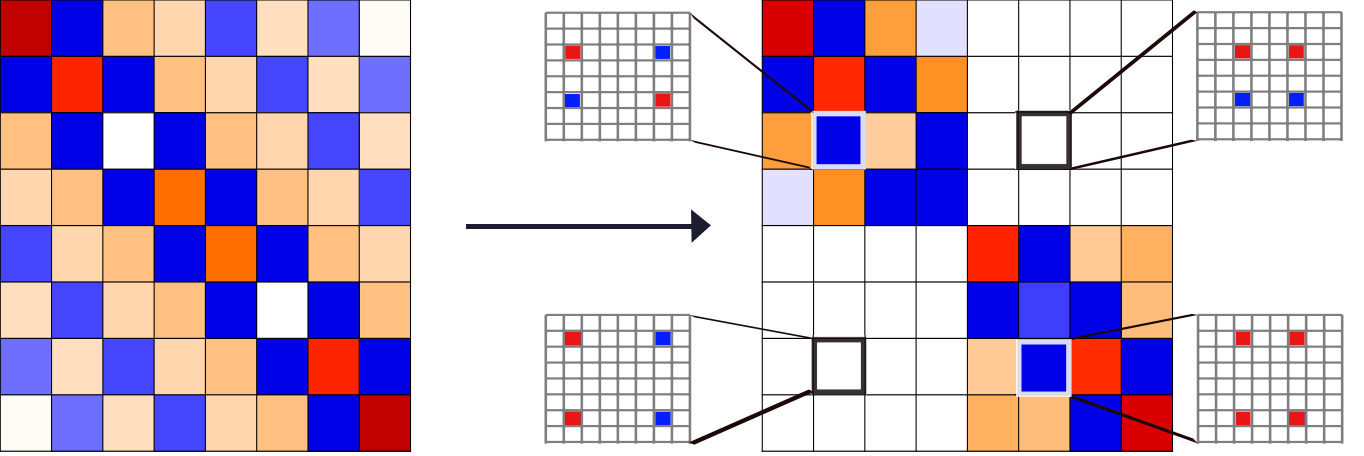


FIG. 7. An illustration of the block-diagonalization ($\tilde{\mathcal{H}}$ on the right) of the nuclear Hamiltonian \mathcal{H} shown on the left as captured by Eq. (12). On the right side, the highlighted matrix elements $\tilde{\mathcal{H}}_{il}$ are obtained from the corresponding elements of \mathcal{H} marked in blue (negative) and the red (positive) colors indicating the phase obtained from the Givens rotation in Eq. (12).

ments: Spin-lattice parameters, $\{B_i^z; J_{ij}^z\}$, are unitary transforms of the diagonal elements of the molecular Hamiltonian: The diagonal elements of the molecular Hamiltonian are directly mapped to those of the spin lattice Hamiltonian after invoking the map of the unitary transformed grid basis to the permuted computational basis. Each diagonal element of the molecular Hamiltonian in the transformed grid representation, $\langle \tilde{x} | \mathcal{H}^{Mol} | \tilde{x} \rangle$, is equivalent to the corresponding element of the ion-trap Hamiltonian, $\langle \lambda | \mathcal{H}_{IT} | \lambda \rangle$ in the permuted computational basis representation, $\{\lambda\}$. In doing so, the set of on-site and inter-site coupling parameters, $\{B_i^z; J_{ij}^z\}$, of the ion-trap that occur along the diagonal of \mathcal{H}_{IT} can be evaluated. The mapping expression between the diagonal elements of the molecular Hamiltonian and the ion-trap Hamiltonian may be written as

$$\langle \tilde{x} | \mathcal{H}^{Mol} | \tilde{x} \rangle \equiv \langle \lambda | \mathcal{H}_{IT} | \lambda \rangle = \sum_{j=1}^N \left\{ (-1)^{\lambda_j} B_j^z + \sum_{k>j}^N (-1)^{\lambda_j \oplus \lambda_k} J_{jk}^z \right\} \quad (13)$$

where \oplus denotes the addition modulo 2, λ denotes the bitwise representation of the computational basis, with λ_j being the j^{th} bit of λ having values 0 or 1 (for up- or down-spin, respectively, see Figure 4). In writing Eq. (13) we have introduced a map between the nuclear wavefunction bases and Ising model bases as:

$$|\lambda\rangle \Leftrightarrow |\tilde{x}\rangle. \quad (14)$$

where $|\lambda\rangle$ is the permuted computational basis that yields the block structure of the Ising Hamiltonian, and $|\tilde{x}\rangle$ is the Givens transformed grid basis. That is, the permuted sequence of computational basis vectors, $|\lambda\rangle$, are mapped, one-to-one, to the Givens transformed grid basis vectors, $|\tilde{x}\rangle$. In Figure 3 in the main paper and Figure 5 in the Methods section, it is the projection of the time-dependent wavepacket on the basis of $|\lambda\rangle$ and $|\tilde{x}\rangle$ that is compared for the 3-qubit problem. In this section we derive general error bounds for an arbitrary number of qubits. Our goal here now is to be able to simulate the diagonal part of $\tilde{\mathcal{H}}^{Mol}$ by tuning the set of ion-trap parameters $\{B_i^z, J_{ij}^z\}$ that determine the diagonal elements of \mathcal{H}_{IT} . As mentioned briefly in the main paper, there is an underlying advantage of the block structure of the two Hamiltonian matrices; it allows us to propagate the two blocks of the Hamiltonian matrices separately. We exploit this to evaluate a set of $\{B_i^z, J_{ij}^z\}$ parameters for each of the diagonal blocks. To this effect, we treat $\{B_i^z, J_{ij}^z\}$ on equal footing and write the mapping expression for the diagonal elements in each block as,

$$\langle \tilde{x} | \mathcal{H}^{Mol} | \tilde{x} \rangle \equiv \langle \lambda | \mathcal{H}_{IT} | \lambda \rangle = \sum_{i=1}^{\frac{N(N+1)}{2}} \mathbf{T}_{\lambda,i} D_i^z \quad (15)$$

where $\{\lambda\}$ corresponds to either of the two sets of computational basis states that independently span $\{\mathbf{S}^{+2n} |11\cdots\rangle\}$ and $\{\mathbf{S}^{+2n-1} |11\cdots\rangle\}$, D^z is a vector that represents in a consolidated fashion, the individual $\{B_j^z, J_{jk}^z\}$ parameters or a linear combination of these parameters and the $\mathbf{T}_{\lambda,i}$ represents a coefficient matrix for the phase preceding the corresponding D_i^z s. The upperlimit for the index i in the above expression thus denotes the maximum number of independent parameters D_i^z s that will encode the diagonal part of $\tilde{\mathcal{H}}^{Mol}$ for a general case of N qubits. Thus, the diagonal elements of the transformed Ising Hamiltonian, $\langle \lambda | \mathcal{H}_{IT} | \lambda \rangle$ encode both the Born-Oppenheimer potential energy surface, $V(x)$, and Givens transformed elements of the nuclear kinetic energy that appear due to block diagonalization process needed to make the two Hamiltonians have the same structure. The transformation matrix on the right side of Eq. (15) with elements, $\mathbf{T}_{\lambda,i} = \pm 1$, represents a selected set of rows from an $N - 1$ -dimensional Hadamard matrix, computed from tensor products of the standard 2×2 (or 1-qubit) Hadamard transform H , that is $H^{\otimes N} \equiv H^{\otimes(N-1)} \otimes H$. Thus, the columns of \mathbf{T} in Eq. (15) are orthogonal and *the D^z values are therefore obtained by an unitary transform of the diagonal elements of the nuclear Hamiltonian*. It is important to note here, that the B^z s and J^z s are combined to obtain the D_i^z parameters, in Eq.(15), in a manner that all rows of the transformation matrix \mathbf{T} remain orthogonal to each other. We, thereby, exploit the orthogonality of the columns of \mathbf{T} to compute the set of parameters $\{B_j^z, J_{jk}^z\}$ for each block of the

N qubit Hamiltonian separately as,

$$D_j^z = \frac{1}{2^{N-1}} \sum_{\{\lambda\}} \mathbf{T}_{j,\lambda} [\mathcal{H}_{IT}]_{\lambda\lambda}. \quad (16)$$

Owing to the equivalence of $\langle \tilde{x} | \mathcal{H}^{Mol} | \tilde{x} \rangle$ and $\langle \lambda | \mathcal{H}_{IT} | \lambda \rangle$, as seen in Eq(14), we use the precomputed diagonal elements of the unitary transformed molecular Hamiltonian in Eq.(15) to compute the on-site parameters of the ion-trap. As per Eq. (13), $\langle \lambda | \mathcal{H}_{IT} | \lambda \rangle$ may be replaced by $\langle \tilde{x} | \mathcal{H}^{Mol} | \tilde{x} \rangle$ in Eq. (17) leading to,

$$D_j^z = \frac{1}{2^{N-1}} \sum_{\{\tilde{x}\} \leftrightarrow \{\lambda\}} \mathbf{T}_{j,\lambda} \langle \tilde{x} | \mathcal{H}^{Mol} | \tilde{x} \rangle \quad (17)$$

where we tersely assume the summation over $\{\lambda\}$ to also correspond to the summation of grid basis vectors as allowed by the correspondence in Eq. (14). The transformation matrix in Eq. (17), that is \mathbf{T}^T , is illustrated in Figure 8 (b and c) for the 2^4 -dimensional sub-blocks of a 5-qubit Ising and for the 2^2 -dimensional sub-blocks of a 3-qubit Ising Hamiltonian in Figure 8 (a). The dimension, $2^{N-1} \times \frac{N(N+1)}{2}$ of the \mathbf{T} matrix is apparent from this figure. The latter dimension of the \mathbf{T} matrix that depends on the number of independent D_j^z s is at most $\frac{N(N+1)}{2}$, and is found to be 3 for the 3-qubit system and 15 for the 5-qubit system. While the figure is only presented for 3-qubit and 5-qubit systems, the transformation is completely general.

At this stage, as already discussed in Eqs. (8) and (9), and by comparison with the upper limit of the summation in Eq. (15), where clearly $\frac{N(N+1)}{2} < 2^{N-1}$ for $N > 4$, it is clear that the number of $\{B_i^z; J_{ij}^z\}$ ion-trap handles are fewer than the number of diagonal elements in the molecular Hamiltonian for large number of qubits. However, it is possible to pre-rotate the molecular Hamiltonian basis so as to compress the amount of information along the diagonal and these aspects will be considered in a future publication.

Arising from the above discussion, the error, ϵ , associated with such a partial Hadamard transform of the diagonal elements of the molecular Hamiltonian can be obtained from the orthogonal complement of the transformation matrix in the corresponding Hadamard matrix. This can be expressed in the closed form as,

$$\epsilon = \frac{1}{2^{N-1}} \sqrt{([\tilde{\mathcal{H}}_{Diag}^{Mol}]^T \mathbf{P}^{\mathbf{T}^{\perp}} [\tilde{\mathcal{H}}_{Diag}^{Mol}]} \quad (18)$$

where $\tilde{\mathcal{H}}_{Diag}^{Mol}$ contains the diagonal elements of $\tilde{\mathcal{H}}^{Mol}$, that is $\langle \tilde{x} | \mathcal{H}^{Mol} | \tilde{x} \rangle$ in the equations above and

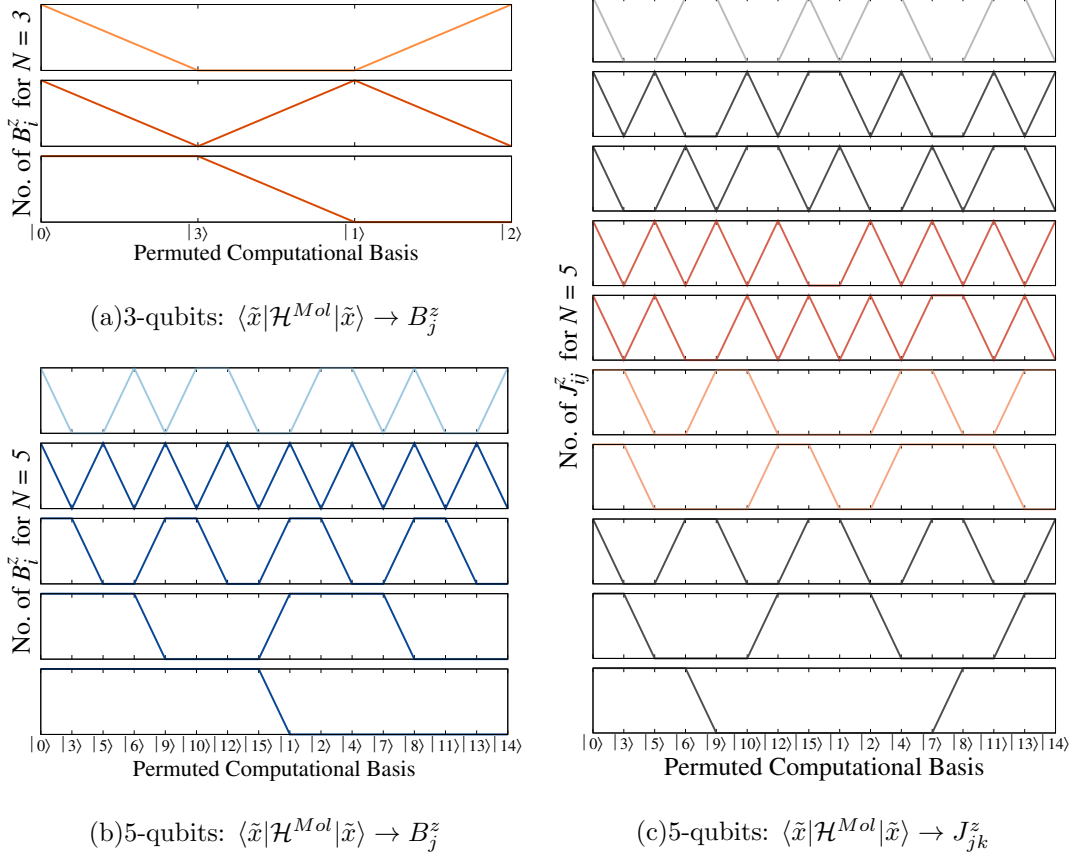


FIG. 8. Figure illustrates the transformation from $\langle \tilde{x} | \mathcal{H}^{Mol} | \tilde{x} \rangle$ to the B^z -values for 3-qubits (a) and B^z (b) and J^z -values (c) for 5-qubits. This inverse matrix picks out the appropriate columns from the 2^{N-1} -dimensional Hadamard transformation matrix. See Eqs. (13) and (17). The B^z transformations (Figures a and b) arise from two basic vectors, (top panel and bottom panel). The vector in bottom panel is scaled in frequency to create the other vectors. This aspect is shown by using two different color shades. Similarly, J^z transformations (Figure c) arise from five basic transformations arranged with different color shades in panels 1-3, 4-5, 6-7, 8-9 and 10.

$\mathbf{P}^{\mathbf{T}^\perp}$ is a projector on to the orthogonal complement of \mathbf{T}

$$\mathbf{P}^{\mathbf{T}^\perp} \equiv 2^{N-1} H^{\otimes(N-1)} H^{\otimes(N-1)T} - \mathbf{T} \mathbf{T}^T = 2^{N-1} \mathbf{I}_{2^{(N-1)}} - \mathbf{T} \mathbf{T}^T \quad (19)$$

is the matrix corresponding to the orthogonal complement of the transformation matrix as obtained from the Hadamard matrix. Thus cases where the diagonal part of the molecular Hamiltonian are exactly captured within the subspace represented by Eq. (17), may be exactly modelled using the ion-trap simulator/computer. In all these cases the orthogonal complement in Eq. (18) is identically zero.

For the 3-qubit case illustrated here, the orthogonal component can be obtained by comparing, the tensor product of two Hadamard matrices,

$$H_2 = \frac{1}{2} \begin{pmatrix} 1 & 1 & 1 & 1 \\ 1 & -1 & 1 & -1 \\ 1 & 1 & -1 & -1 \\ 1 & -1 & -1 & 1 \end{pmatrix} \quad (20)$$

and

$$[\mathbf{T}]^T = \begin{pmatrix} 1 & -1 & -1 & 1 \\ 1 & -1 & 1 & -1 \\ 1 & 1 & -1 & -1 \end{pmatrix} \quad (21)$$

to arrive at the first row vector of Eq. (20). This row is the zero-frequency component or the average of the diagonal elements of the molecular Hamiltonian and, therefore, simply results in a uniform shift of the diagonal elements. This results in a constant shift between the eigenvalues of the molecular Hamiltonian and the Ising Hamiltonian, which results in no change in the dynamics, as is clear from Figures 3, 5 and 6.

Author Contributions

The theory behind the mapping protocols were developed by DS, SSI, PR and AS. The formalism to evaluate the symmetries embedded within the Ising model and expose the block structure was developed by DS and SSI. Computer program development, electronic structure potential surface calculations, and quantum molecular dynamics calculations were performed by DS. Validation of vibrational properties were studied by DS, SSI and JMS. All authors contributed to the writing of the manuscript.